Eur. Phys. J. A **30**, 603–611 (2006)
DOI 10.1140/epja/i2006-10136-3

THE EUROPEAN PHYSICAL JOURNAL A

An experiment for the measurement of the bound-β-decay of the free neutron

W. Schott[1], G. Dollinger[2], T. Faestermann[1], J. Friedrich[1], F.J. Hartmann[1,a], R. Hertenberger[3], N. Kaiser[1], A.R. Müller[1], S. Paul[1], and A. Ulrich[1]

[1] Physik Department, Technische Universität München, D-85748 Garching, Germany
[2] Institut für Angewandte Physik und Messtechnik, Universität der Bundeswehr München, D-85577 Neubiberg, Germany
[3] Sektion Physik der Ludwig-Maximilians-Universität München, D-85748 Garching, Germany

Received: 14 February 2006 / Revised: 6 September 2006 /
Published online: 4 December 2006 –
Communicated by Th. Walcher

Abstract. The hyperfine-state population of hydrogen after the bound-β-decay of the neutron directly yields the neutrino left-handedness or a possible right-handed admixture and possible small scalar and tensor contributions to the weak force. Using the through-going beam tube of a high-flux reactor, a background free hydrogen rate of ca. $3\,\mathrm{s}^{-1}$ can be obtained. The detection of the neutral hydrogen atoms and the analysis of the hyperfine states is accomplished by Lamb shift source type quenching and subsequent ionization. The constraints on the neutrino helicity and the scalar and tensor coupling constants of the weak interaction can be improved by a factor of ten.

PACS. 13.30.Ce Leptonic, semileptonic, and radiative decays – 14.20.Dh Protons and neutrons

1 Introduction

The neutron decay is for many years the subject of intense studies, as it reveals detailed information about the structure of the weak interaction. However, the studies have so far only addressed the main decay channel (classical neutron three-body β-decay), where decay rates and decay asymmetries have been determined with great precision [1]. Symmetries of the interaction are accessible by the precise measurement of momentum spectra of the decay products and/or their correlation with the neutron spin alignment. In addition, experiments are planned, where the polarization of the final-state particles (electron or proton) is measured. However, there is a very elegant method to measure very precisely the relative spin alignments of the daughter products and their correlation. Using the two-body neutron β-decay into a hydrogen atom (H) and an electron antineutrino ($\bar{\nu}$),

$$n \rightarrow \mathrm{H} + \bar{\nu}, \tag{1}$$

one can investigate the hyperfine population of the emerging hydrogen atom. The challenge lies in the very small branching ratio $BR = 4{\cdot}10^{-6}$ of the total neutron β-decay rate [2], which is the result of the small phase space for the efficient coalescence necessary for H formation. We expect only states with zero angular momentum in the hydrogen atom to be populated; these are mainly the $1s$ and the metastable $2s$ states with 83.2% and 10.4% probability, respectively. This is because states of angular momentum $l > 0$ have a negligible expectation value in the center of the potential. The residual 6.4% ns states with $n > 2$ decay within nanoseconds, mainly into the $1s$ state. At a first stage of the experiment, only 10% of the bound-β-decay H can be used for the proposed $2s$ state spin analysis. The $2s$ H rate may be increased by $1s \rightarrow 2s$ excitation (cf. below).

Using the standard V-A theory the possible spin configurations emerging from this bound-β-decay emitted hydrogen atom are given in table 1.

According to [3] for a purely left-handed V-A interaction, the population probabilities W_i of the first three configurations i can be deduced to be

$$W_1 = \frac{(\chi-1)^2}{2(\chi^2+3)}\,, \tag{2}$$

$$W_2 = \frac{2}{\chi^2+3}\,, \tag{3}$$

$$W_3 = \frac{(\chi+1)^2}{2(\chi^2+3)}\,, \tag{4}$$

depending only on one variable $\chi = (1+g_S)/(\lambda - 2g_T)$, with $\sum_{i=1}^{3} W_i = 1$. λ is the ratio

$$\lambda = g_A/g_V = -1.2695 \pm .0029\ [1].$$

[a] e-mail: joachim.hartmann@ph.tum.de

Table 1. Spin projections i in the neutron bound-β-decay. As a convention, H moves to the right, $\bar{\nu}$ to the left. Fe and GT mean Fermi and Gamov-Teller transition, respectively. W_i are the populations according to the pure V-A interaction (cf. eqs. (2)-(4) of ref. [2]), F the total spin (with hyperfine interaction) and m_F the F projection, $|m_S m_I\rangle$ the Paschen-Back state, where m_S and m_I denote the e^- and p spin quantum numbers (+means +1/2, *i.e.* spin points to the right in the magnetic quantization field direction). The population probability W_i is $W_i = N_i/N$ with N_i being the configuration i state population and $N = \sum_{i=1}^{3} N_i$.

Configuration i	$\bar{\nu}$	n	p	e^-	Transition	$W_i(\%)$	F	m_F	$\|m_S m_I\rangle$
1	$\leftarrow$	$\leftarrow$	$\leftarrow$	$\rightarrow$	Fe/GT	44.14 ± 0.05	0,1	0	$\|+-\rangle$
2	$\leftarrow$	$\leftarrow$	$\rightarrow$	$\leftarrow$	GT	55.24 ± 0.04	0,1	0	$\|-+\rangle$
3	$\leftarrow$	$\rightarrow$	$\rightarrow$	$\rightarrow$	Fe/GT	0.622 ± 0.011	1	1	$\|++\rangle$
4	$\rightarrow$	$\leftarrow$	$\leftarrow$	$\leftarrow$	Fe/GT	0.0	1	-1	$\|--\rangle$
$2'$	$\rightarrow$	$\rightarrow$	$\rightarrow$	$\leftarrow$	Fe/GT	0.0	0,1	0	$\|-+\rangle$
$1'$	$\rightarrow$	$\rightarrow$	$\leftarrow$	$\rightarrow$	GT	0.0	0,1	0	$\|+-\rangle$

Table 2. $W_i(\%)$ for various g_S and g_T.

Configuration i	$g_S = 0$ $g_T = 0$	$g_S = 0.1$ $g_T = 0$	$g_S = 0$ $g_T = 0.02$
1	44.14	46.44	43.40
2	55.24	53.32	55.82
3	0.622	0.238	0.780
4	0.0	0.0	0.0

g_A, g_V, g_S, g_T are the axial, vector, scalar and tensor coupling constants, respectively. Thus, by means of W_i only a combination of g_S and g_T can be measured. g_S is obtained from W_i only if g_T is known from somewhere else and vice versa.

The V-A contribution to the emission of H in one of its hyperfine spin states with $F = 1$ and $m_F = 1$ (configuration 3 of table 1) is suppressed by about two orders of magnitude (cf. eq. (4)). Therefore, by measuring the population of this configuration in relation to the configurations 1 and 2 (both $m_F = 0$), the existence of S, P, T weak interaction variants can be verified. While the states $F = 1$, $m_F = \pm 1$ (configurations 3 and 4) are pure eigenstates of the Hamiltonian describing the p-e^- interaction in an external magnetic field B_1, linear combinations of the configuration 1 and 2 states with coefficients depending on B_1 yield the other two eigenstates. Therefore, the configurations 3 and 4 are separated in any case from configurations 1 and 2, whereas a separation of configurations 1 and 2 is only possible, if the decays occur within a magnetic field B_1 (cf. below).

The sensitivity of W_i with respect to g_S and g_T is shown in table 2 [3], where the W_i are calculated assuming small admixtures of g_S and g_T.

The last three configurations 4, $1'$ and $2'$ in table 1 cannot be populated by a left-handed V-A interaction, but only by emission of right-handed neutrinos. Among these configurations, only configuration 4, namely $|--\rangle$, is a pure hyperfine energy state, see eq. (5). Among the other configurations, $1'$ is mixed with 2, and $2'$ is mixed with 1, see eqs. (8) and (10) and cannot be studied separately.

A possible small contribution of negative helicity to $\bar{\nu}$ would manifest itself by a non-zero value of W_4 in table 1. The population of configuration 4, predicted by a left-right symmetric V+A model, is given by [4]

$$W_4 = \frac{(x + \lambda y)^2}{2(1 + 3\lambda^2 + x^2 + 3\lambda^2 y^2)}\,, \tag{5}$$

with $x = \eta - \zeta$ and $y = \eta + \zeta$, where η is the mass ratio squared of the two intermediate charged vector bosons and ζ the boson mass eigenstate mixing angle, η and ζ being $\eta < 0.036$ [5] and $|\zeta| < 0.03$ (C.L. 90%) [6], respectively. In this model the antineutrino helicity $H_{\bar{\nu}}$ becomes

$$H_{\bar{\nu}} = \frac{1 + 3\lambda^2 - x^2 - 3\lambda^2 y^2}{1 + 3\lambda^2 + x^2 + 3\lambda^2 y^2}\,. \tag{6}$$

The neutron decay is then mediated by right-handed currents, the details of which are absorbed in η and ζ. The best data for neutrino helicities come from τ and μ decay spectra and the extraction of the Michel parameters. Typical accuracies are on the order of 15% [7]. Similar accuracies can be achieved using the B-coefficient in neutron decay [8].

A certain background to the configurations 1–4, $1'$, $2'$ comes from s states with larger principal quantum number n, also originally populated. These ns states with $n > 2$ subsequently decay into the $1s$ and $2s$ states by spontaneous emission of photons, where the spin quantum number m_S of e^- is changed. If only the $2s$ state is used for the spin analysis, the $4s$ and higher-state population yield a $2s$ background slowly converging with n; as an example $W(4s \to 2s) = 3.07 \cdot 10^{-4}$ and $W(5s \to 2s) = 2.18 \cdot 10^{-4}$ (cf. appendix). From the sum $W(4s \to 2s) + W(5s \to 2s) = 5.25 \cdot 10^{-4}$ a fraction of 44.2% (that is $2.32 \cdot 10^{-4}$) would contribute to configuration 4 as background, and 55.2% of the sum ($2.90 \cdot 10^{-4}$) would show up in configuration 3. The latter background constitutes already 47% of the resulting W_3 rate, which, according to $W(2s) \cdot W_3$, contributes $6.2 \cdot 10^{-4}$ to the $2s$ population.

In order to improve the present g_S, g_T and $H_{\bar{\nu}}$ accuracies (cf. below), the background due to optical m_S changing transitions from ns states with $n > 2$ into the $2s$ state analyzed must be eliminated, *e.g.* by ionizing these ns H atoms using a laser prior to their decay.

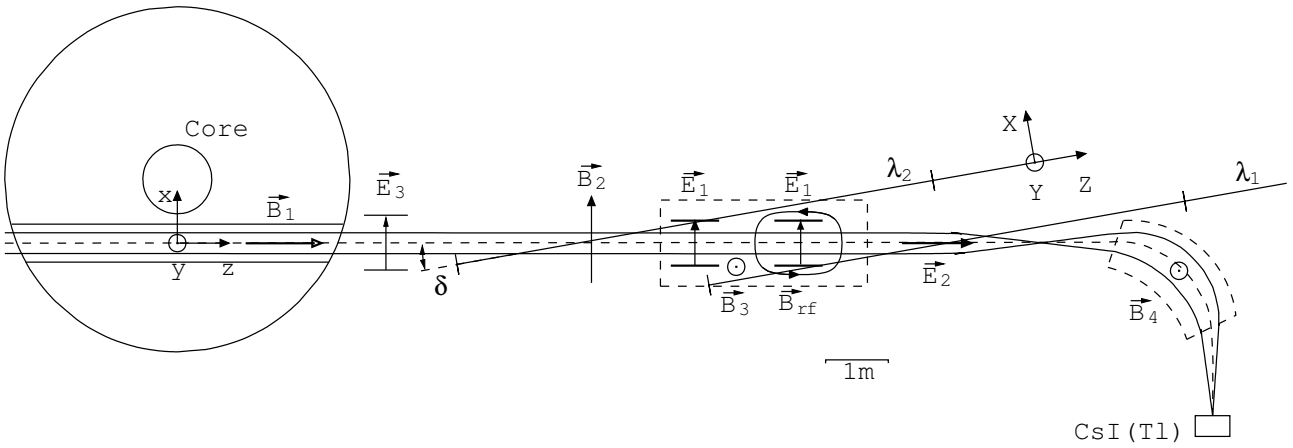

Fig. 1. Sketch of the experimental setup for measuring hydrogen atoms from bound-β-decay at FRMII. The through-going beam tube with the magnetic quantization field $\mathbf{B}_1$ and a transverse electric field $\mathbf{E}_3$ for deflecting and suppressing the neutron-β-decay protons are drawn. The analyzing station starts with a field $\mathbf{B}_2$ by means of which the spin is rotated by $\pi/2$, followed by a level splitting field $\mathbf{B}_3$ with a transverse electric field $\mathbf{E}_1$ and a transverse rf magnetic field $\mathbf{B}_{\rm rf}$ inside, a longitudinal accelerating and focussing electric field $\mathbf{E}_2$ and a bending and focussing magnetic field $\mathbf{B}_4$, where $\mathbf{B}_2 \| \ x$ or $-x$, $\mathbf{B}_3 \| \ y$, $\mathbf{E}_1 \| \ x$, $\mathbf{B}_{\rm rf}$ in the z-x plane. By means of the $\lambda_2 = 243\,\mathrm{nm}$ and the $\lambda_1 = 364\,\mathrm{nm}$ laser the H atoms are excited from $1s$ to $2s$ and ionized, respectively. The reflecting mirrors of the two laser resonators are indicated by bars. Alternatively, the ionization from the $2s$ state can be achieved by a $2s$ to $3p$ and a consecutive $3p$ to continuum excitation using for the first step a $\lambda_1 = 656\,\mathrm{nm}$ laser superimposed, *e.g.*, by an intense 816 nm light source beam ($364^{-1}\,\mathrm{nm}^{-1} = 656^{-1}\,\mathrm{nm}^{-1} + 816^{-1}\,\mathrm{nm}^{-1}$). The resulting protons are detected using a small CsI(Tl) crystal.

2 Experiment

Figure 1 depicts the suggested setup to perform a neutron bound-β-decay experiment. Hydrogen atoms from this decay have a kinetic energy of $T_{\rm H} = 326.5\,\mathrm{eV}$, which corresponds to a velocity v with $v/c = 0.83 \cdot 10^{-3}$. They are produced in the high neutron flux from an intense neutron source and extracted from a through-going beam pipe. In the following we will assume a high-flux neutron beam from the FRMII reactor. Different possibilities for such a neutron source will be discussed below.

The proposed setup of observing the emerging hydrogen atom parallel to a magnetic field has the virtue that we automatically define a helicity axis which coincides with the quantization axis for the various HFS states. On the opposite side, the neutrino helicity axis follows from angular-momentum conservation. We thus do not need to operate with polarized neutrons (see table 1). At the same time we can reverse the direction of the quantization axis by operating the system with reversed B fields. This will become important when discussing the spin analysis of the emerging hydrogen by means of Paschen-Back splitting in a strong field.

The B field in the decay volume is also necessary for a second reason, which at the same time defines its minimum strength. In order to preserve the magnetic quantum numbers of the electron and of the proton, m_S and m_I, (also in the case of total spin $F = 0$), the Zeeman coupling to the external fields must be larger than the HFS coupling within the hydrogen atom. The latter one corresponds to an internal magnetic field of 507 gauss (63.4 gauss) for the $1s(2s)$ levels, also called the critical field B_c [9] (B_c is the magnetic field of the electron at the position of the proton, which causes the hyperfine splitting (fig. 2)). Thus the field in the decay volume should exceed the value of 63.4 gauss, since the $2s$ level splitting is used.

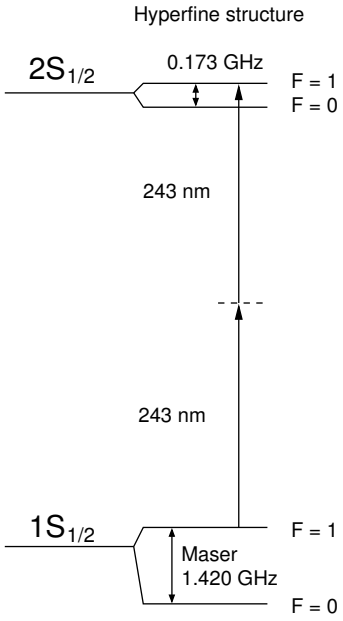

Fig. 2. Hyperfine splitting of the $1s$ and $2s$ state of hydrogen.

During their passage in the beam tube the hydrogen atoms move to the right, the hyperfine spin states $F = 1$, $m_F = 0, \pm 1$ or $|m_S m_I\rangle$ states are kept in a longitudinal magnetic quantization field B_1, which extends from the neutron decay volume to the analyzing station starting from the $\mathbf{B}_2$ field. $\mathbf{B}_1$ is produced by a long solenoid

with an iron yoke outside the reactor covering part of the magnetic return flux path. There is an intermediate field region between $\mathbf{B}_1$ and $\mathbf{B}_2$ such that $\mathbf{B}_1$ is non-zero before $\mathbf{B}_2$ rises. Neutron-β-decay protons are deflected and suppressed by the transverse electric field $\mathbf{E}_3$ (ca. 4 kV/m) outside the through-going beam pipe.

2.1 Spin analysis and detection of 326.5 eV H atoms

The hyperfine analyzing part starts with a transverse magnetic field

$$B_2 = \hbar\pi v/(2\mu_B \delta z_2) = 10\,\text{gauss},$$

where μ_B is the Bohr magneton and $\delta z_2 = 4.4$ mm the extension of the $\mathbf{B}_2$ field region within which the $2s$, $F = 1$, $m_F = 0, \pm 1$ states are rotated adiabatically by $\pi/2$ into the same states, however, with the quantization axis being perpendicular to the direction of flight and parallel to the magnetic field $\mathbf{B}_3$ with $B_3 \approx 575$ gauss, immediately following the $\mathbf{B}_2$ field region. $\mathbf{B}_2$ is produced by a long solenoid. The solenoid with an iron yoke is large in x-direction, thus, having a negligible stray field. The intermediate field region between $\mathbf{B}_2$ and $\mathbf{B}_3$ is such that $\mathbf{B}_2(z)$ is non-zero before the stray field $\mathbf{B}_3(z)$ rises. Therefore, the $\mathbf{B}_2$ solenoid is positioned close to the $\mathbf{B}_3$ magnet. The distance in z-direction between both is about the gap width of the $\mathbf{B}_3$ dipole magnet of 0.13 m being the side length a of a cube shaped $\nu = 1.609$ GHz TE101 mode cavity ($a = c/(\sqrt{2}\cdot\nu)$). The $\mathbf{B}_3$ magnet can be C-shaped with iron poles and an iron yoke.

Figure 3 depicts the Breit-Rabi diagram of the $2s_{1/2}$ hyperfine states in a magnetic field, also showing the corresponding $2p_{1/2}$ states [9].

The α and β states are related to the $|m_S m_I\rangle$ states as

$$\alpha(1,1) = |++\rangle, \tag{7}$$
$$\alpha(1,0) = \cos\theta|+-\rangle + \sin\theta|-+\rangle, \tag{8}$$
$$\beta(1,-1) = |--\rangle, \tag{9}$$
$$\beta(0,0) = \sin\theta|+-\rangle - \cos\theta|-+\rangle, \tag{10}$$

where θ is given by $\tan 2\theta = B_c/B$ with the quantization field B and the critical field B_c. Indicated are the states $\alpha(F, m_F)$ etc.

If there exists a magnetic field $\mathbf{B}_1$ in the through-going beam tube at the point of neutron decay, the $\alpha(1,0)$ and $\beta(0,0)$ population of the hydrogen atoms from bound-β-decay is given by

$$N_{\alpha 10} = N_1 \cos^2\theta + N_2 \sin^2\theta \tag{11}$$

and

$$N_{\beta 00} = N_1 \sin^2\theta + N_2 \cos^2\theta \tag{12}$$

with N_1 and N_2 being the configuration $1(|+-\rangle)$ and $2(|-+\rangle)$ state population from table 1, respectively. Thus, $\alpha(1,0)$ and $\beta(0,0)$ are not equally populated if the bound-β-decays occur in a magnetic field $B_1 \neq 0$ (and, thus, $\theta \neq \pi/4$). This population is conserved up to the region of spin analysis (with $\mathbf{B}_3$ field) if no level transitions are induced. χ can be obtained by measuring the ratios $v_{\alpha\beta} = N_{\alpha 10}/N_{\beta 00}$ or $v_{\alpha\alpha} = N_{\alpha 11}/N_{\alpha 10}$.

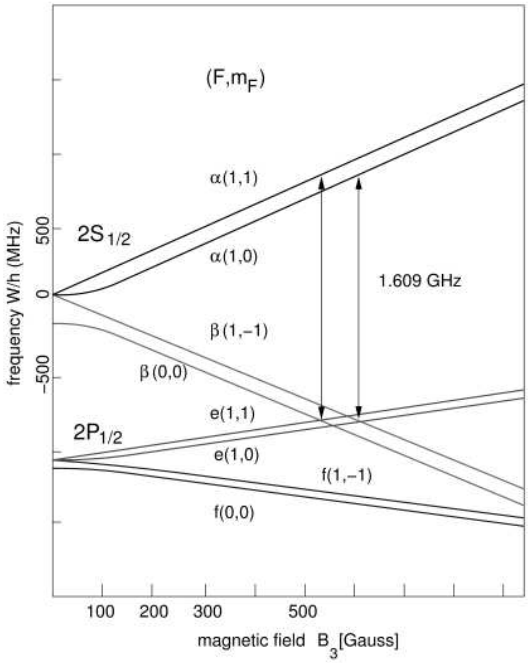

Fig. 3. Breit-Rabi diagram of the hyperfine splitting of the $2s_{1/2}$ and $2p_{1/2}$ states in a magnetic field, where $W = -(g_I m_I - g_j m_S)\mu_B B_3$ is the energy, g_I and g_j the p and e^- gyromagnetic factors and μ_B the Bohr magneton, respectively [9].

At the presence of only $\mathbf{B}_3$, the β and e states are degenerate. With $\mathbf{B}_3$, an electric field $\mathbf{E}_1$ and an rf field $\mathbf{B}_{\text{rf}}$ this degeneracy is removed resulting in two B_3 fields, where the $\alpha\,\beta\,e$ states couple. Owing to Stark mixing in an electric field superimposed transversely to B_3, the states $\beta(1,-1)$ and $\beta(0,0)$, originally metastable, can mix with the $e(1,0)$ and $e(1,1)$ states. Using $E_1 = 4.3$ V/cm, the lifetime τ_β of the β states is thus strongly reduced ($v\cdot\tau_\beta = 1.1$ cm) as compared to the lifetime τ_α of the α states ($v\cdot\tau_\alpha = 1.8\cdot 10^3$ cm) [2]. An electric field E_1 of about 100 V/cm would also reduce $v\cdot\tau_\alpha$ to about 1 cm.

Thus, in the $\mathbf{E}_1 \times \mathbf{B}_3$ field the $2s_{1/2}$, $F = 1$, $m_F = -1$ and the $2s_{1/2}$, $F = 0$ states are quenched immediately, decaying back into the respective $1s_{1/2}$ ground state, whereas the two $2s_{1/2}$ states with $F = 1$, $m_F = 1$ and $F = 1$, $m_F = 0$ survive.

One of the two remaining α states can be selected by the spin filter method using the simultaneous interaction of the α, β and e levels at B_3 [9,10]. Owing to the static transverse electric field $\mathbf{E}_1$ (fig. 1), β and e are mixed. Then, we apply an rf field of 1.609 GHz, causing the α states to interact with the coupled β-e levels. At $B_3 \approx 538$ gauss the $\alpha(1,0)$ will be quenched and the $\alpha(1,1)$ state will be selected, whereas with the same frequency at $B_3 \approx 605$ gauss the $\alpha(1,0)$ will remain, and the $\alpha(1,1)$ will be removed. If the quantizing field $\mathbf{B}_1$ is

reversed, $\alpha(1,1)$ will be replaced by $\beta(1,-1)$ and $\alpha(1,0)$ by $\beta(0,0)$, respectively. The transmission curve for a single spin state is 0.4 gauss wide because of the width of the perturbed β state [9,11]. Therefore, for a perfect separation of the spin states, B_3 must be homogeneous to ± 0.2 gauss. The rf field can be produced within a box-shaped cavity in the TE101 mode, yielding $\mathbf{B}_{\rm rf}$ field lines perpendicular to $\mathbf{B}_3$ (fig. 1) surrounding the cavity center y-axis corresponding to an rf electric field in the $\mathbf{B}_3$ direction and, thus, causing α-β transitions. Because of the β-e mixing required at the position of $\mathbf{B}_{\rm rf}$, the static $\mathbf{E}_1$ field must be implemented within the cavity.

As discussed in the introduction, the detection of a population of configuration 4 from table 1, which feeds the state $\beta(1,-1)$, is of eminent importance. The spin filter must thus be operated such that only the $|--\rangle$ configuration survives, requiring a full quenching of the α states. This can be achieved by operating the experiment with reversed fields. The magnetic level splitting will thus be reversed in sign, where $\beta(1,-1)$ becomes $\alpha(1,1)$ and $\beta(0,0)$ becomes $\alpha(1,0)$, respectively (however, we will keep the nomenclature defined in the Rabi diagram of fig. 3). A depopulation of the two β states requires a passage of the H atoms through a varying magnetic field with crossed E field. When passing the fields of 538 and 605 gauss, Stark mixing will cause a depopulation of the corresponding $2s$ states. We are left with the two α states. We then pass through the same filter as before operated at a field of 538 gauss and a transition laser frequency of 1.609 GHz. This will cause a transition between $\alpha(1,1)$ and $\beta(0,0)$ with subsequent quenching. We will be left with the desired configuration $|--\rangle$ (table 1) which can be identified as before through ionization and proton detection. Proton detection comes later on in the text.

As the accuracy required is extremely large (zero measurement at a level of 10^{-6}–10^{-7}), we must take care of false effects. Some of them are listed below.

- Inefficient depopulation of the unwanted HFS states.
- Atomic cascades from ns states (with $n > 2$) which may feed $2s$ via an intermediate p state in an uncontrolled way. See the appendix for details.
- Radiative effects: additional soft photons may distort our arguments on angular-momentum conservation and lead to a population of np states (with $n > 2$). This can be calculated in the framework of radiative corrections.

Downstream of the cavity and the $\mathbf{B}_3$ field the remaining state-selected H atoms (*e.g.*, $2s_{1/2}$, $F = 1$, $m_F = 1$) are ionized by, *e.g.*, a $\lambda_1 = 364$ nm laser beam (fig. 1). Alternatively, the ionization may be driven by an optical two-step process, using, *e.g.*, a $2s \rightarrow 3p$ transition ($\lambda = 656.28$ nm) and subsequent ionization by a high-power laser ($\lambda = 816.33$ nm) or an incoherent light source of that wavelength. The produced protons are accelerated by an electrostatic field $\mathbf{E}_2$ to about 20 keV energy and focussed to a small spot on the beam axis, from where they are deflected by 90° by an analyzing magnetic field $\mathbf{B}_4$ and transported by point-to-point imaging onto a CsI(Tl) scintillator. Using a photomultiplier to detect the light output

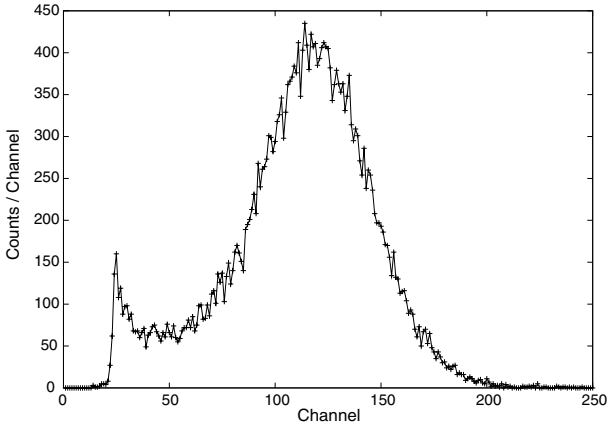

Fig. 4. Pulse-height spectrum from 18.5 keV protons measured with a 1 cm^3 cubic CsI(Tl) crystal and a photomultiplier.

the protons can be detected with high efficiency as demonstrated in a test experiment, where 18.5 keV protons have been measured (fig. 4). The magnetic field $\mathbf{B}_4$ provides radial and axial focussing of the proton beam owing to 22.5° entrance and exit edge angles. The drift lengths l_0 and l_1 before and after the $\mathbf{B}_4$ magnet with radius of curvature ρ are related to first order by [12]

$$\rho = \frac{\pi}{4} l_0 \left(-1 + \sqrt{1 + \frac{8}{\pi}} \right), \tag{13}$$

$$l_1 = l_0 \frac{\pi}{4} \left(1 + \frac{\pi}{2} - \sqrt{1 + \frac{8}{\pi}} \left(\frac{\pi}{2} - 1 \right) \right). \tag{14}$$

One interesting addition would be an intense $\lambda_2 = 243$ nm laser beam crossing the beam line at an angle $\delta = 100$ mrad for exciting the H atoms from $1s$ to $2s$ by means of two-λ_2 photon absorption (fig. 2). Although not considered in the present context, this pumping station would allow to use about 50% of all hydrogen atoms produced in the subsequent hyperfine analysis, as compared to the 10.4% H atoms from direct $2s$ population, the basis for all following rate discussions. However, no high-power Lyman-α laser is presently available.

In order to suppress the configuration 1–4 background due to ns states with $n > 2$, the corresponding H atoms can be ionized by a $\lambda = 816.33$ nm laser with resonators positioned at both ends of the experiments straight section, *i.e.* at the left end of the through-going beam tube (fig. 1) and behind the $\mathbf{E}_2$ focus.

2.2 Possible event rates

In the following we will evaluate possible event rates. We will assume the setup, as depicted in fig. 1, to be installed at the new Munich high-flux reactor FRMII. Extrapolations to other neutron sources will be derived at the end.

The neutron decay volume within the beam pipe SR6 of the FRMII has a length $l = 2 \cdot z_S$, with $z_S = 4.7$ m and a radius $r_S = 0.0715$ m. z_S is the distance between the

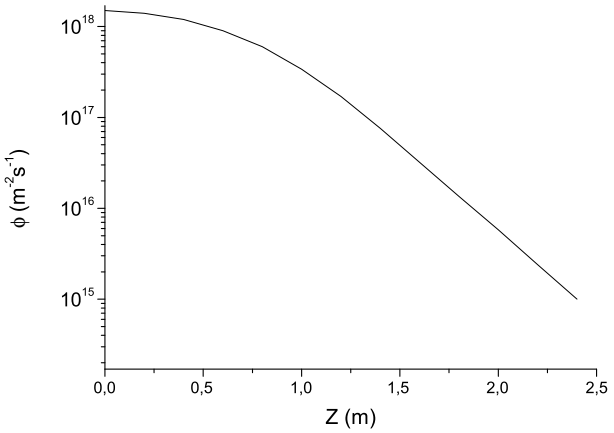

Fig. 5. Thermal neutron flux along the FRMII SR6 through-going beam tube.

center and the far end of SR6. The expected H rate $\dot{N}_{\rm H}$ at one exit of this beam pipe, at a distance $z_S = 4.7\,{\rm m}$ from its center (fig. 1), is given by

$$\dot{N}_{\rm H} = BR \cdot \int (\Phi(z)\Omega_S(z){\rm d}V)/4\pi \cdot 1/\tau_n \cdot 1/v_n, \quad (15)$$

where $\tau_n = 886\,{\rm s}$ is the neutron lifetime, $\Phi(z)$ the thermal neutron flux along the SR6 z-axis (fig. 5) [13,14], V the SR6 volume, $\Omega_S = A_S/z_S^2$ the solid angle of the hydrogen spectrometer, with $A_S = 0.01\,{\rm m}^2$ being the spin filter, *i.e.*, the TE101 cavity acceptance cross-section. $v_n = 2.2 \cdot 10^3\,{\rm m/s}$ is the average thermal-neutron velocity. Thus, the integral can be written as

$$(1/4\pi) \int \Phi(z)\Omega_S(z){\rm d}V = \frac{A_S}{2} \left(\frac{r_S}{z_S}\right)^2 \int_0^{z_s} \Phi(z){\rm d}z. \quad (16)$$

$\dot{N}_{\rm H} = 3\,{\rm s}^{-1}$ is obtained using the thermal neutron flux distribution of refs. [13,14] (fig. 5). According to eqs. (15) and (16), the neutron density N_n/V, *i.e.* the number of neutrons N_n in the observed SR6 volume V, is given by

$$N_n/V = \int_0^{z_S} (\Phi(z){\rm d}z)/(v_n\, z_S) = 2.4 \cdot 10^8\,{\rm cm}^{-3},$$

being about $3{\cdot}10^4$ times larger than the ultra-cold neutron (UCN) density in the recently proposed UCN sources, *e.g.* ref. [15].

2.3 Expected experimental constraints on g_S, g_T and $H_{\bar{\nu}}$

A small g_S or g_T contribution including the sign may be measured via the population probability W_3. In [16] a 1σ confidence level upper limit for the absolute value of g_S is quoted to be $g_S \leq 6{\cdot}10^{-2}$. In order to obtain for $g_T = 0$ an assumed value for $g_S = 6{\cdot}10^{-2}$ with the same accuracy using the bound-β-decay, the statistical error $(\delta W_3)_{\rm stat}$ must be 1σ, where σ is the standard deviation. Using eq. (4) and the value of λ, the difference

$$\begin{aligned} \Delta W_3 = |&W_3(g_S = 6 \cdot 10^{-2}, g_T = 0) \\ &- W_3(g_S = 0, g_T = 0)| = 2.54 \cdot 10^{-3} \end{aligned}$$

can be written as

$$\Delta W_3 = (\delta W_3)_{\rm stat} + 2\,|(\delta W_3)_\lambda|\,, \quad (17)$$

where $(\delta W_3)_{\rm stat}$ is the statistical error, and $(\delta W_3)_\lambda$ the uncertainty due to the error on λ. Using $\delta\lambda = 2.9{\cdot}10^{-3}$ [1], we obtain

$$(\delta W_3)_\lambda = ({\rm d}W_3/{\rm d}\lambda)\delta\lambda = -1.10 \cdot 10^{-4}. \quad (18)$$

Hence, for measuring $W_3(g_S = 6 \cdot 10^{-2}, g_T = 0) = 3.68 \cdot 10^{-3}$ with 68% confidence, $(\delta W_3)_{\rm stat} = 2.32 \cdot 10^{-3}$ corresponds to 1σ. W_3 can be written as

$$W_3 = \frac{N_3}{N}\,, \quad (19)$$

with

$$N = \sum_{i=1}^{3} N_i \quad (20)$$

the total number of counts and N_i the individual number of counts for configuration i, respectively. σ is then

$$\sigma \approx \frac{\sqrt{N_3}}{N} \quad (21)$$

yielding

$$N = \frac{W_3}{\sigma^2} = 684. \quad (22)$$

The measuring time required is

$$t = \frac{N}{\dot{N}} \quad (23)$$

with $\dot{N} = \dot{N}_{\rm H}$. If all hydrogen atoms from bound-β-decay moving along the beam tube were considered, t becomes about 228 s. As only the $2s_{1/2}$ states can be used (see the discussion above) with $\dot{N} \approx 0.1\,\dot{N}_{\rm H}$, the necessary time to confirm the present $g_S = 6 \cdot 10^{-2}$ upper limit is 2280 s.

The statistical error for g_S can be written as

$$\begin{aligned} (\delta g_S)_{\rm stat} &= \left| \left(\frac{\partial g_S}{\partial W_3}\right)_{g_S = 6{\cdot}10^{-2},\, g_T = 0} \right| \cdot (\delta W_3)_{\rm stat} \\ &= \left| \frac{\lambda(\chi^2+3)^2}{-\chi^2+2\chi+3} \right| \cdot \sqrt{\frac{W_3}{N}} \end{aligned}$$

with $(\delta g_S)_{\rm stat} = 6{\cdot}10^{-3}$ ($\chi \approx 1/\lambda, W_3 = 3.683{\cdot}10^{-3}$), $N = 4.4{\cdot}10^4$ results, which corresponds to 40 h measuring time (${\rm d}N_{\rm H}/{\rm d}t = 3\,{\rm s}^{-1}$), when only the $2s_{1/2}$ state is used. This reduces the present g_S upper limit by a factor of ten.

Assuming a finite detection efficiency ϵ, these times scale with the factor $1/\epsilon$. Since $\epsilon \geq 0.1$ seems to be realistic, the g_S upper limit could be lowered by a factor of ten within a few weeks of measuring time.

According to eqs. (5) and (6) with $\zeta = 0$, *i.e.*, $x = y = \eta$, W_4 and $H_{\bar{\nu}}$ are approximately given by [4]

$$W_4 \approx \frac{\eta^2(1+\lambda)^2}{2(1+3\lambda^2)}\,, \tag{24}$$

$$H_{\bar{\nu}} \approx 1 - 2\eta^2 = 1 - \frac{4(1+3\lambda^2)}{(1+\lambda)^2} \cdot W_4. \tag{25}$$

The statistical error of $H_{\bar{\nu}}$ becomes

$$(\delta H_{\bar{\nu}})_{\mathrm{stat}} = \frac{4(1+3\lambda^2)}{(1+\lambda)^2} \cdot \sqrt{\frac{W_4}{N}}\,. \tag{26}$$

Assuming $\eta = 0.036$, we obtain $W_4 = 8.1 \cdot 10^{-6}$ and $H_{\bar{\nu}} = 0.997$. This yields $N = 8.3 \cdot 10^3$ for $(\delta H_{\bar{\nu}})_{\mathrm{stat}} = 1 \cdot 10^{-2}$, *i.e.* 8 h measuring time using only the $2s_{1/2}$ state.

2.4 Observables for χ

χ is given by the ratios $v_{\alpha\beta}$ or $v_{\alpha\alpha}$, defined in sect. 2.1, according to eqs. (2) to (4) and (11) to (12),

$$v_{\alpha\beta} = \frac{(\chi-1)^2\cos^2\theta + 4\sin^2\theta}{(\chi-1)^2\sin^2\theta + 4\cos^2\theta}\,, \tag{27}$$

$$v_{\alpha\alpha} = \frac{(\chi+1)^2}{(\chi-1)^2\cos^2\theta + 4\sin^2\theta}\,, \tag{28}$$

with χ either

$$\chi = 1 \pm 2\sqrt{\frac{\sin^2\theta - v_{\alpha\beta}\cos^2\theta}{v_{\alpha\beta}\sin^2\theta - \cos^2\theta}}\,, \tag{29}$$

or

$$\chi = \frac{-(1+v_{\alpha\alpha}\cos^2\theta) \pm 2\sqrt{v_{\alpha\alpha}(1 - v_{\alpha\alpha}\sin^2\theta\cos^2\theta)}}{1 - v_{\alpha\alpha}\cos^2\theta}\,. \tag{30}$$

If g_S and g_T are small, the "−" sign holds in eq. (29) and the "+" sign holds in eq. (30).

2.5 Necessary power of the lasers

The ionization of $2s$ hydrogen atoms can be obtained in a two-step process. The excitation from the $2s$ to the $3p$ state by a $\lambda_1 = 656.28$ nm laser beam (fig. 1) is selective to the moving H atoms from bound-β-decay because of the Doppler shift. The consecutive ionization can be achieved by an intense incoherent 816.33 nm light source. The necessary power $\dot{Q}_1$ in the λ_1 laser resonator is given by

$$\dot{Q}_1 = j_1\, E_1\, \delta X\, \delta Y. \tag{31}$$

j_1 is the photon current density, $E_1 = 1.889$ eV the photon energy, $\delta X = 0.3$ mm and $\delta Y = 0.1$ m the λ_1 laser-beam waist width in X- and Y-direction, respectively, completely covering the H beam with the dimensions $\delta x = \delta y = 0.1$m.

The λ_1 and λ_2 laser beams, both having these δX and δY dimensions, are produced within resonators, each consisting of two reflectors which are small in X-direction and large in Y-direction. The laser beams coupled into the resonators are widened in Y-direction. The resulting resonator modes can be considered to be formed by two waves travelling in opposite Z-directions, where only one wave can be used for the Doppler-shift selected laser spectroscopy, *e.g.*, to excite H from $2s$ to $3p$. Since the quality of the resonators can be large, the power of the laser beams coupled into the resonators is only a small fraction of the laser power within the resonators.

The requested photon current j_1 can be written as

$$j_1 = -\frac{\ln(1-P_1)}{\sigma_1\, \Delta t}\,, \tag{32}$$

where $P_1(2s \to 3p)$ is the desired $2s \to 3p$ excitation probability, σ_1 the $2s \to 3p$ photon-absorption cross-section and Δt the exposure time, $\Delta t = \delta X/(v\,\delta) = 12$ ns, since $\sin\delta \approx \delta$. v is the neutron decay hydrogen atom velocity and $\delta = 100$ mrad the λ_1 laser resonator inclination with respect to the beam axis z. σ_1 is given by

$$\sigma_1 = \frac{\lambda^3 A_{ik}}{8\pi c}\left(\frac{\lambda}{\mathrm{d}\lambda}\right) = 5.08 \cdot 10^{-16}\,\mathrm{m}^2, \tag{33}$$

with the Einstein transition coefficient [17]

$$A_{ik} = \frac{6.67 \cdot 10^{13} \cdot f_{ik}}{(\lambda(\mathrm{nm}))^2}\,, \tag{34}$$

where the oscillator strength f_{ik} is $f_{ik} = 0.641$ for the $2s \to 3p$ transition [18]. The λ_1 laser resonator quality $\lambda_1/\mathrm{d}\lambda_1$ is matched to the relative width $\mathrm{d}\lambda_1/\lambda_1$ which is necessary because of the Doppler broadening $\mathrm{d}\lambda_1$ caused by the thermal motion of the decaying neutron, $\mathrm{d}\lambda/\lambda = v_n/c = 0.73 \cdot 10^{-5}$. The Doppler shift $\Delta\lambda$ renders a high selectivity against thermally moving H with $\Delta\lambda/\lambda = 0.83 \cdot 10^{-3}$. A laser power $\dot{Q}_1 = 2.4$ W is needed for $P_1 = 0.8$.

In order to reduce the background from the population of higher ns states in the neutron decay, a minimum power for an ionization laser with $\lambda = 816.33$ nm of $\dot{Q}_1 = 216.7$ W covering the production volume is required, as may be derived using eqs. (31) to (34). Considering W_4, the efficiency for the removal has to be $P_1 = 1$–$8.1 \cdot 10^{-7}$, thus closer to one by one order of magnitude than the value of $W_4 = 8.1 \cdot 10^{-6}$ to be measured (cf. subsect. 2.3). We assume $\mathrm{d}\lambda/\lambda = 0.73 \cdot 10^{-5}$, the oscillator strength $f \approx 1$ for the transition $n \geq 3$ into the continuum [18], the lifetime of the $3s$ state $\Delta t = \tau(3s) = 158.4$ ns, the photon energy $E_1 = 1.512$ eV and the waist widths $\delta x = \delta y = 0.1$ m.

At present, we have only considered H atoms in the $2s$ state. A much improved count rate could be obtained when also the $1s$ hydrogen atoms could be used which make up 83% of the resulting hydrogen final states. However, this requires a pumping of all $1s$ to $2s$ states of the hydrogen atoms before entering the spin selector. This can in principle be achieved by means of a UV laser

beam crossing the hydrogen path under a small angle δ (cf. fig. 1). The $1s \rightarrow 2s$ transition requires a two-photon process. We estimated $P(1s \rightarrow 2s)$ from the ionization probability $P(1s \rightarrow \text{continuum})$, which has been calculated for the three-photon process by [19].

The photon density for the two-photon absorption must be large, requiring a small λ_2 laser beam waist δX (fig. 1). δX is limited by the uncertainty relation, constraining the λ_2 laser beam angular width within the resonator to be $\delta\Theta \geq \lambda_2/(2\pi\delta X)$, yielding $\delta\Theta \geq 0.13\,\text{mrad}$ for a technically feasible beam waist $\delta X = 0.3\,\text{mm}$ and the resonator length $(2\delta X/\delta\Theta)$ to be less than 4.6 m. The passage time Δt of the H atoms through the λ_2 laser resonator inclined by $\delta = 100\,\text{mrad}$ with respect to the beam z-axis is 12 ns.

The necessary power density I_2 for the $1s$-to-$2s$ transition in the λ_2 laser resonator may be estimated from the calculated ionization probability $P(1s \rightarrow \text{continuum}) = 6.5 \cdot 10^{-4}$ for a λ_2 laser pulse with $\Delta t = 10\,\text{fs}$ duration and $I_2 = 5 \cdot 10^{12}\,\text{W/cm}^2$ [19]. Assuming $P(1s \rightarrow \text{continuum}) = (C_1 \cdot I_2 \cdot \Delta t)^3$, $C_1 = 1.73 \cdot 10^{-4}\,\text{s}^2/\text{kg}$ results. $P_2 = P(1s \rightarrow 2s)$ should be given as $P_2 = (C_1 \cdot I_2 \cdot \Delta t)^2$, yielding $I_2 = 1.66 \cdot 10^7\,\text{W/cm}^2$ for $P_2 = 0.1$ and $\Delta t = 12\,\text{ns}$. The high power density is at the present technical limit for a continuous beam covering an area of $\delta X \cdot \delta Y = 0.3\,\text{mm} \cdot 100\,\text{mm} = 30\,\text{mm}^2$.

2.6 Background suppression

The fast hydrogen atoms from the bound-β-decay of the neutron, emitted to the right-hand side of fig. 1, are observed through collimators outside the through-going beam pipe. The collimators have to be placed such that the wall of the inner tube is not visible by the detectors, because backscattered neutralized protons from normal β-decays would produce a huge background. The setup also minimizes the neutron flux at the end of the beam tube. The protons emitted to the left are deflected by electric or magnetic fields such that they do not hit the back end of the beam tube, where they could be backscattered and neutralized producing a background flux of H atoms in the analyzing direction. High-vacuum conditions ($\leq 10^{-6}\,\text{hPa}$) are also recommended to avoid neutralization of protons from three-body neutron decay and to avoid scattering of the H atoms from bound-β-decay. The background, *i.e.* the probability P_3 for neutron or proton scattering at the rest gas atoms in the beam-tube vacuum should be less than 1%. P_3 is given by $P_3 = \sigma_3\, n_3\, \Delta z \leq 10^{-2}$, where $\sigma_3 = 10^{-16}\,\text{cm}^2$ is a typical scattering cross-section, n_3 the atom density of the rest gas and $\Delta z = 10\,\text{m}$ the vacuum chamber length, yielding $n_3 \leq 10^{11}\,\text{cm}^{-3}$: the beam line vacuum should be better than $4.1 \cdot 10^{-4}\,\text{Pa}$.

3 Conclusion

In this manuscript we outline an experiment to determine the scalar and tensor contribution to the weak interaction including their signs as well as the constraints on the left-handedness of the neutrino with ten times higher precision than the present value. Currently, the upper limit on g_S is $|g_S| \leq 6 \cdot 10^{-2}$ (C.L. 68%) [16], whereas $|g_T/g_A| \leq 0.09$ (C.L. 95%) [20]. From the measurements of neutron β-decay asymmetry coefficients upper limits for the left-handed and right-handed boson mass squared and the absolute value of the boson mixing angle are determined to be $\eta < 0.036$ [5] and $|\zeta| < 0.03$ (C.L. 90%) [6], respectively. In the proposed experiment the upper limits of g_S or g_T and η or ζ can be reduced by a factor of ten.

The issue is addressed by measuring the spin correlation between the proton and the electron. They are defined with respect to their direction of flight (measuring direction) by selecting different hyperfine states from the bound-β-decay of the neutron. Although the experimental requirements are challenging, we show a pathway to perform such an experiment at the through-going beam tube of a high-flux reactor like the FRMII. Slightly better conditions do exist at the corresponding beam tube of the high-flux reactor in Grenoble, as the usable neutron density is about four times higher [21]. Next generations of spallation neutron sources like the SNS may be even better suited, if a through-going beam tube is provided, since higher neutron densities are expected and the pulsed neutron beam makes the detection of hydrogen atoms and the background suppression easier.

We are especially grateful to Prof. J. Byrne for carefully reading the manuscript and many valuable comments. We also want to thank Dr A. Röhrmoser for calculating the neutron and gamma flux in the FRMII SR6 beam tube.

Appendix A.

The most important contribution from higher excited states of hydrogen to the $2s$ hyperfine states are given by the contribution to $W(4s \rightarrow 2s)$ changing m_S. This may be written as

$$\begin{aligned} W(4s \rightarrow 2s) &= 2 \cdot W(4s) \cdot W(4s \rightarrow 3p) \cdot W(3p \rightarrow 2s) \\ &\quad \cdot W(\Delta j = 0) \cdot W(\Delta j = \pm 1) \\ &= 3.07 \cdot 10^{-4}, \end{aligned}$$

where $W(4s) = 1.3\%$ is the original $4s$ population.

$$W(4s \rightarrow 3p) = A_{4s3p}/(A_{4s3p} + A_{4s2p}) = 0.416 \quad \text{and}$$
$$W(3p \rightarrow 2s) = A_{3p2s}/(A_{3p2s} + A_{3p1s}) = 0.118$$

is the $4s \rightarrow 3p$ and $3p \rightarrow 2s$ transition probability, respectively. A_{4s3p} is the corresponding $4s \rightarrow 3p$ Einstein transition coefficient [17]. The factor two arises from the interchangability of the time-ordered transitions with $\Delta j = 0$ and $\Delta j = \pm 1$. Assuming the two transition probabilities for the e^- spin quantum number m_S (m_S changing with $\Delta j = 0$ and m_S non-changing with $\Delta j = \pm 1$) to be equal, where $j = l + s$ is the spin orbit coupling realized, the probability for $\Delta j = 0$ and $\Delta j = \pm 1$ photons of the $p \rightarrow s$

transition is given by the multiplicities of the Zeeman-split p and s levels. They are $W(\Delta j = 0) = 2/5$ and $W(\Delta j = \pm 1) = 3/5$.

Correspondingly, the m_S changing background contribution from the $5s$ state is given by

$$\begin{aligned} W(5s \to 2s) &= 2 \cdot W(\Delta j = 0) \cdot W(\Delta j = \pm 1) \cdot W(5s) \\ &\quad \cdot [W(5s \to 4p) \cdot W(4p \to 2s) \\ &\quad + W(5s \to 3p) \cdot W(3p \to 2s)] \\ &= 2.18 \cdot 10^{-4} \end{aligned}$$

with $W(5s) = 0.7\%$,

$$\begin{aligned} W(5s \to 4p) &= A_{5s4p}/(A_{5s4p} + A_{5s3p} + A_{5s2p}), \\ W(4p \to 2s) &= A_{4p2s}/(A_{4p2s} + A_{4p3s} + A_{4p1s}), \\ W(5s \to 3p) &= A_{5s3p}/(A_{5s3p} + A_{5s4p} + A_{5s2p}) \quad \text{and} \\ W(3p \to 2s) &= A_{3p2s}/(A_{3p2s} + A_{3p1s}). \end{aligned}$$

References

1. S. Eidelman *et al.*, Phys. Lett. B **592**, 1 (2004) and partial update for edition 2006.
2. L.L. Nemenov, Sov. J. Nucl. Phys. **31**, 115 (1980).
3. L.L. Nemenov, A.A. Ovchinnikova, Sov. J. Nucl. Phys. **31**, 659 (1980).
4. J. Byrne, Eur. Phys. Lett. **56**, 633 (2001).
5. A. Gaponenko *et al.*, Phys. Rev. D **71**, 071101 (2005).
6. J.R. Musser *et al.*, Phys. Rev. Lett. **94**, 101805 (2005).
7. SLD Collaboration (K. Abe *et al.*), Phys. Rev. Lett. **78**, 4691 (1997).
8. I.A. Kuznetsov *et al.*, Phys. Rev. Lett. **75**, 794 (1995).
9. W. Haeberli, Annu. Rev. Nucl. Sci. **17**, 373 (1967) and references quoted therein.
10. W.E. Lamb, R.C. Retherford, Phys. Rev. **79**, 549 (1950).
11. F.-J. Eckle, Diploma thesis, Sektion Physik der Universität München (1982).
12. C. Bovet *et al.*, CERN/MPS-SI/Int. DL/70/4, 23 April 1979, p. 12.
13. W. Gaubatz, Technische Universität München (TUM), private communication.
14. I. Altarev *et al.*, internal report, TUM (2000).
15. U. Trinks *et al.*, Nucl. Instrum. Methods **440**, 666 (2000).
16. E.G. Adelberger *et al.*, Phys. Rev. Lett. **83**, 1299 (1999).
17. W.L. Wiese *et al.*, in Natl. Stand. Ref. Data Ser., Natl. Bur. Stand. **4**, Category 3 - Atomic and Molecular Properties (1966).
18. K. Omidvar, A.M. McAllister, Phys. Rev. A **51**, 1063 (1995).
19. M. Roth *et al.*, HMI Annual Report (2001) p. 20.
20. A.I. Boothroyd, J. Markey, P. Vogel, Phys. Rev. C **29**, 603 (1984).
21. E.G. Kessler *et al.*, Nucl. Instrum. Methods A **457**, 187 (2001).